Materials Research Proceedings 33 (2023) 294-300 https://doi.org/10.21741/9781644902677-43

An extended ordinary state-based peridynamics model for ductile fracture analysis

Jing Zhang[1,2,a], Qingsheng Yang[1*], Xia Liu[1 *]

[1] Department of Engineering Mechanics, Beijing University of Technology

[2] MUL2 Group, Politecnico di Torino

[a] zh_jing@emails.bjut.edu.cn

Keywords: Peridynamics, Meshfree Method, Elastoplastic Deformation, Fracture

Abstract. The present research establishes a two-step strategy to incorporate classical elastoplastic constitutive model into ordinary state-based peridynamics (OSB-PD) for ductile fracture analysis. Three length levels are notified, respectively, bond level, material particle level and bulk level. The unified Bodner-Partom theory is incorporated into the OSB-PD framework to define the bond-wise relationship between deformation state and force state. Particle-wise variables indicating plastic deformation state are extracted from connecting bonds to establish the unified ductile damage model at particle level. The damage indicator in turn exerts effects on the following plastic deformation. At present study, the collaboration among PD and unified theories amplifies the theoretical unity of PD in defining material behaviors. Simulations under quasi-static and impact loading conditions are carried out to demonstrate the effectiveness of the present model in reproducing ductile fractures at bulk level.

Introduction

Ductile fracture is a non-trivial issue, accompanied by high plastic deformation, that affects the workability of engineering materials [1]. During plastic deformation, with the proliferation of dislocations and the emergence of voids and cracks, the amplified effects of material inhomogeneity and discontinuity can influence the computational accuracy and efficiency [2]. Therefore, nonlocal meshfree methods like smoothed particle hydrodynamics (SPH) and reproducing kernel particle method (RKPM) are utilized to describe the phenomena where long-range interactions affect the global behavior of the solution. However, it is inevitable to deal with spatial derivatives or their approximations during dynamic crack propagation [3]. Special treatments for fracture and fragmentation are still needed to accommodate the emergence of new free surfaces. To eliminate these concerns, peridynamics (PD) theory reformulates the classical continuum mechanics (CCM) into an integral-differential form with no spatial derivatives required [4].

Originated from molecular dynamics, PD concerns the nonlocal effects of material particles within a certain cutoff distance named horizon. With the newly-proposed “state” instead of tensor, PD establishes a general version of CCM, making it mathematically compatible with crack initiation and propagation without any complementary numerical treatments [5]. PD can then provide a unified formulation of for nonlocal theories including SPH, CSPH, RKPM, G-RKPM and it has been successfully applied on the failure analysis of rocks, metals, polymers and composites [6]. The constitutive models are expressed as the relations between force state and deformation state. They can be carefully divided into two categories concerning ordinary state-based PD (OSB-PD) and non-ordinary state-based PD (NOSB-PD), according to the geometrical relations between force state and deformation state. To describe ductile fracture, PD has been collaborated with numerous constitutive models from different length scales [7], concerning

Materials Research Proceedings 33 (2023) 294-300 https://doi.org/10.21741/9781644902677-43

Johnson-Cook theory, Comacho and Ortiz theory, crystal plasticity theory, Gurson-Tvergaard-Needleman theory, Multiscale Micromorphic Molecular Dynamics theory, *etc*.

However, most of the developed PD models concentrate on a certain stage of deformation. The yield surface needs to be defined additionally for plastic deformation, which undermines the theoretical unity of PD theory. The present paper aims to define a unified elastoplastic model coupled with ductile damage to describe the full-course ductile fracture process in a unified manner. The Bodner-Partom (BP) theory [8] is modified to collaborate with OSB-PD theory, while Wang's ductile damage theory [9,10], in a unified manner akin to the BP theory, works along with the modified BP theory and functions as a material deterioration indicator. Final fracture is predicted using a critical bond stretch criterion due to its effectiveness and computational stability. The present elastoplastic model is carefully verified through numerical simulations.

The remainder of this study is threefold. Section 2 introduces the extended elastoplastic OSB-PD theory and the two-step implementation strategy. Multiple verification tests under various loading conditions are conducted in Section 3. Main conclusions and future works are summarized in Section 4.

Theory

A PD body B_0 moves to B_t with a certain deformation. The material body is discretized into numerous material particles. Each central particle possesses a spherical neighborhood $H_{\mathbf{x}}$ with a radius of δ, named horizon. Within the horizon, central particle $\mathbf{x}$ generates bonds with its neighbor particles $\mathbf{x}'$. In OSB-PD, material response at a point depends on the collective deformation of all connecting bonds. PD equations of motion are given by [5]

$$\rho(\mathbf{x})\ddot{\mathbf{u}}(\mathbf{x},t) = \int_{H_{\mathbf{x}}} \{\underline{\mathbf{T}}[\mathbf{x},t]\langle\mathbf{x}'-\mathbf{x}\rangle - \underline{\mathbf{T}}[\mathbf{x}',t]\langle\mathbf{x}-\mathbf{x}'\rangle\} dV_{\mathbf{x}'} + \mathbf{b}(\mathbf{x},t) \tag{1}$$

where ρ is mass density in the reference configuration; $\mathbf{u}$ is the displacement vector field; $\mathbf{b}$ is the prescribed body force field; $V_{\mathbf{x}'}$ is the volume of particle $\mathbf{x}'$; $\underline{\mathbf{T}}[\mathbf{x}',t]\langle\mathbf{x}'-\mathbf{x}\rangle$ is the force vector state of particle $\mathbf{x}'$ contributed by bond $\mathbf{x}'-\mathbf{x}$ at time t.

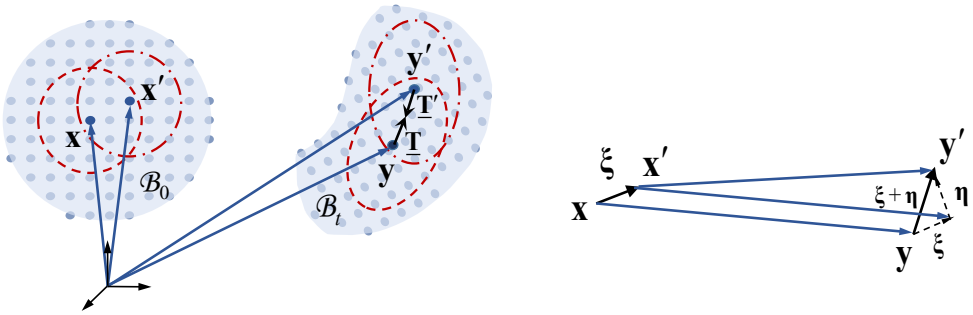

Fig. 1 PD kinematics.

Bond $\boldsymbol{\xi} = \mathbf{x}' - \mathbf{x}$ is also known as the reference position vector state $\underline{\mathbf{X}}[\mathbf{x},t]\langle\boldsymbol{\xi}\rangle$ of particle $\mathbf{x}$ at time t. It is mapped to the deformed configuration as a deformation vector state $\underline{\mathbf{Y}}[\mathbf{x},t]\langle\boldsymbol{\xi}\rangle = \mathbf{y}(\mathbf{x}',t) - \mathbf{y}(\mathbf{x},t) = \boldsymbol{\xi} + \boldsymbol{\eta}$. The displacement vector state $\boldsymbol{\eta}$ is written as $\underline{\mathbf{U}}[\mathbf{x},t]\langle\boldsymbol{\xi}\rangle = \mathbf{u}(\mathbf{x}',t) - \mathbf{u}(\mathbf{x},t)$. The extension scalar state $\underline{e}$ is defined as

$$\underline{e} = \underline{y} - \underline{x} \tag{2}$$

where $\underline{y} = |\underline{\mathbf{Y}}|$, $\underline{x} = |\underline{\mathbf{X}}|$. It can be decomposed into an isotropic part $\underline{e}^{\mathrm{i}} = \frac{\theta \underline{x}}{3}$ and a deviatoric part $\underline{e}^{\mathrm{d}} = \underline{e} - \underline{e}^{\mathrm{i}}$. The volume dilatation is defined as $\theta = \frac{3}{m}(\underline{\omega}\underline{x}) \bullet \underline{e}$, where m is the weighted volume defined as $m = (\underline{\omega}\underline{x}) \bullet \underline{x}$; $\underline{\omega}(\|\boldsymbol{\xi}\|) = \frac{1}{\|\boldsymbol{\xi}\|}$ is a spherical influence function for isotropic materials.

For plastic deformation, deviatoric extension state $\underline{e}^{\mathrm{d}}$ is further decomposed into an elastic part $\underline{e}^{\mathrm{de}}$ and a plastic part $\underline{e}^{\mathrm{dp}}$. In consideration of plastic incompressibility, the extension state $\underline{e}$ can be expressed as

$$\underline{e} = \underline{e}^{\mathrm{i}} + \underline{e}^{\mathrm{de}} + \underline{e}^{\mathrm{dp}} \tag{3}$$

where p is PD pressure defined as $p = -k\theta$. The plastic deformation follows the modified Prandtl-Reuss rule. The rate form of plastic bond extension is expressed as

$$\dot{e}^{\mathrm{dp}} = \frac{R_0}{\sqrt{J_{2\mathrm{s}}}} \exp\left[-\left(\frac{n_{\mathrm{BP}}+1}{2n_{\mathrm{BP}}}\right)\left(\frac{Z^2}{3J_{2s}}\right)^{n_{\mathrm{BP}}}\right] \underline{t}^{\mathrm{d}} \cdot \underline{x} \tag{4}$$

where $J_{2\mathrm{s}}$ is defined as $J_{2\mathrm{s}} = \frac{1}{2}\underline{t}^{\mathrm{d}}\underline{t}^{\mathrm{d}}$; Z is a history-dependent variable representing the material hardening state, defined as $Z = Z_1 - (Z_1 - Z_0)e^{-m_{\mathrm{BP}}W^{\mathrm{p}}}$. W^{p} is an equivalent bond-wise plastic work; $R_0, Z_0, Z_1, m_{\mathrm{BP}}, n_{\mathrm{BP}}$ are material parameters. Then the force scalar state $\underline{t}$ is given by

$$\underline{t} = \underline{t}^{\mathrm{i}} + \underline{t}^{\mathrm{d}} = -\frac{3p}{m}\underline{\omega}\underline{x} + \alpha\omega\left(\underline{e}^{\mathrm{d}} - \underline{e}^{\mathrm{dp}}\right) \tag{5}$$

The unified ductile damage is defined at material particle level to measure the isotropic damage degree. A two-step strategy is hereby proposed to connect elastoplastic deformation and ductile damage. The elastoplastic deformation status extracted from bond level can manifest the degree of material damage, while the damage indicator $\bar{D}$ computed from particle level, in turn, exerts impacts on the following development of plastic deformation through bond-wise damage indicator D. The PD equation of motion coupled with damage is then modified as

$$\rho(\mathbf{x})\ddot{\mathbf{u}}(\mathbf{x},t) = \int_{H_{\mathbf{x}}}(1-D)\{\underline{\mathbf{T}}[\mathbf{x},t]\langle\mathbf{x}'-\mathbf{x}\rangle - \underline{\mathbf{T}}[\mathbf{x}',t]\langle\mathbf{x}-\mathbf{x}'\rangle\}\mathrm{d}V_{\mathbf{x}'} + \mathbf{b}(\mathbf{x},t) \tag{6}$$

where $D = \frac{\bar{D}+\bar{D}'}{2}$ takes an average between the damage values of particle $\mathbf{x}'$ and $\mathbf{x}$. The evolution of D can be described by Wang's unified damage theory

$$\bar{D} = \bar{D}_0 + \frac{\bar{D}_{\mathrm{c}} - \bar{D}_0}{k_{\mathrm{D}}(\bar{s}_{\mathrm{c}} - \bar{s}_0)^{\alpha_{\mathrm{D}}}}\left[(\bar{s}_{\mathrm{c}} - \bar{s}_0)^{\alpha_{\mathrm{D}}} - \left[\bar{s}_{\mathrm{c}} - f^{1/\alpha_{\mathrm{D}}}\left(\frac{\bar{\sigma}^{\mathrm{m}}}{\bar{\sigma}^{\mathrm{eq}}}\right)\bar{s}^{\mathrm{p}}\right]^{\alpha_{\mathrm{D}}}\right] \tag{7}$$

$$f\left(\frac{\bar{\sigma}^{\mathrm{m}}}{\bar{\sigma}^{\mathrm{eq}}}\right) = \frac{2}{3}(1+\nu) + 3(1-2\nu)\left(\frac{\bar{\sigma}^{\mathrm{m}}}{\bar{\sigma}^{\mathrm{eq}}}\right)^2 \tag{8}$$

where $\bar{D}_0, \bar{D}_{\mathrm{c}}, \bar{s}_0, \bar{s}_{\mathrm{c}}, \alpha_{\mathrm{D}}, k_{\mathrm{D}}$ are material constants. k_{D}, among others, is defined for smoothing over the discrepancy between bond-wise damage intensity and bulk damage intensity. $\bar{s}^{\mathrm{p}}$ denotes plastic bond stretch; $\bar{\sigma}^{\mathrm{m}}$ denotes PD pressure, which functions as a measure of isotropic expansion; $\bar{\sigma}^{\mathrm{eq}}$ is PD equivalent stress [11]. The complete logic of the present model is illustrated in Fig. 2.

Materials Research Proceedings 33 (2023) 294-300 https://doi.org/10.21741/9781644902677-43

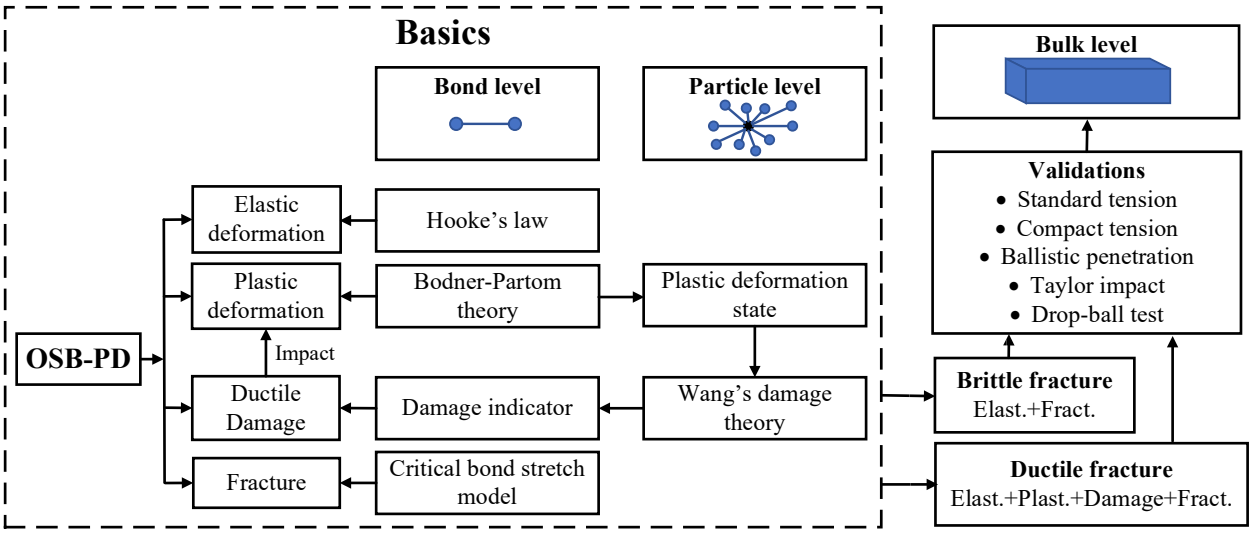

Fig. 2 theory basics.

Main results

This section aims to exploit the effectiveness of the extended OSB-PD constitutive model in predicting the natural development of plastic deformation and material failure. Simulations under quasi-static and high-velocity loading conditions are conducted, including standard tension tests, compact tension (CT) tests and Taylor impact (TI).

A series of standard tension tests are conducted on aluminum alloy 6061(T6) dog-bone specimens for model validation [1,12]. Three aspects are carefully discussed, concerning the effects of model constituents, model applicability on specimens with different degrees of non-uniformity and rate sensitivity effects. The strain-hardening effect is introduced by internal variable Z from the BP theory. The damage model functions as a counterpart to the strain-hardening variable by introducing a material deterioration factor with effect throughout all deformation stages. The bond deterioration further contributes to the collective description of material degradation, leading to the slightly downward trend in simulation curves. By integrating and coordinating all the constituents, satisfactory simulation result can be obtained. Specimens with higher degree of geometrical non-uniformity show better performances than those uniform ones. It indicates that the current computational model cannot deal with massive yielding situations. Numerical instabilities occur near the end of the deformation process, which are translated as severe fluctuations, even collapse, of the simulation curve. Moreover, the modelling results of standard tension tests under different loading rates show a good agreement to experiment data. The fitting degree were satisfactory with little fluctuations at the beginning of plastic flow, which is caused by the stiffness problem of BP theory.

Materials Research Proceedings 33 (2023) 294-300 https://doi.org/10.21741/9781644902677-43

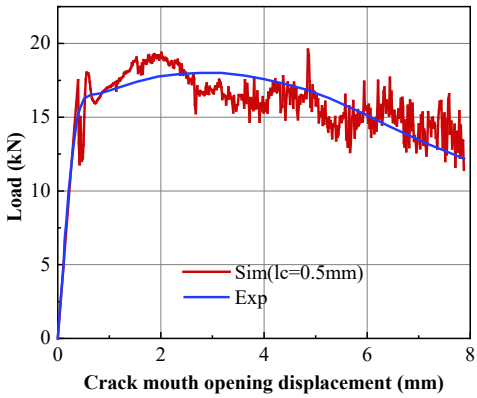

Fig. 3 Load vs. Crack mouth opening displacement curves

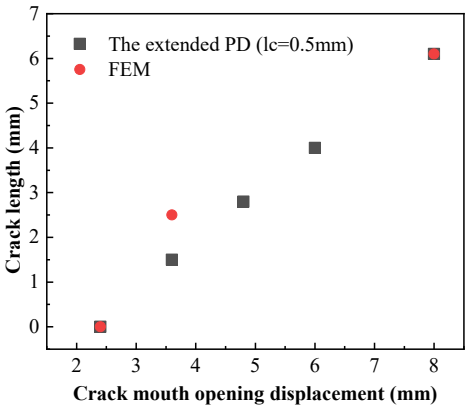

Fig. 4 Crack length vs. Crack mouth opening displacement curves

The compact tension test [13] is carried out to show the capability of the present model in describing crack propagation behaviors. The test material was DH36 steel with Young's modulus of 210 GPa and the Poisson's ratio of 0.3. The PD model was discretized into 467376 particles in simple cubic structure with the lattice constant (lc) of 0.5 mm. The horizon was 1.5 mm. A quasi-static displacement boundary condition was enforced on two cylinders with a diameter of 6.35 mm along y-axis. The total displacement of 8.0 mm was finished within 89000 steps. According to Fig. 3, the simulation curve obtained by the present PD model (red) follows a similar trend to that of the experiment curve (blue). Oscillations can be noticed during the deformation, which attributes to the effects of sudden bonding and bond breakage. Two sets of synchronic cloud charts, showing the intensity of plastic deformation and crack propagation path, are presented in Table 1. The crack grows steadily and clearly. Around the crack tip there is an enlarging elliptical plastic zone. When the discretization degree attains plane-wise 3904 pixels, corresponding to the lattice constant of 0.5 mm, the simulation results are believed trustful according to Fig. 4.

Table 1 The distribution of plastic deformation and crack propagation path (lc=0.5mm)

		Crack mouth opening displacements				
		2.4mm	3.6mm	4.8mm	6mm	8mm
Middle plane	Intensity of plastic deformation	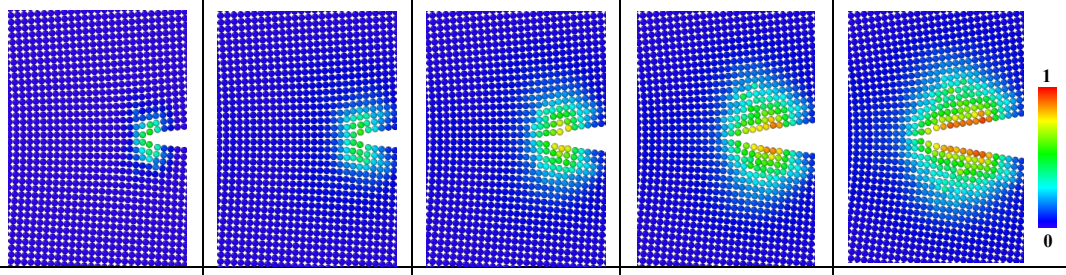				
	Fracture degree	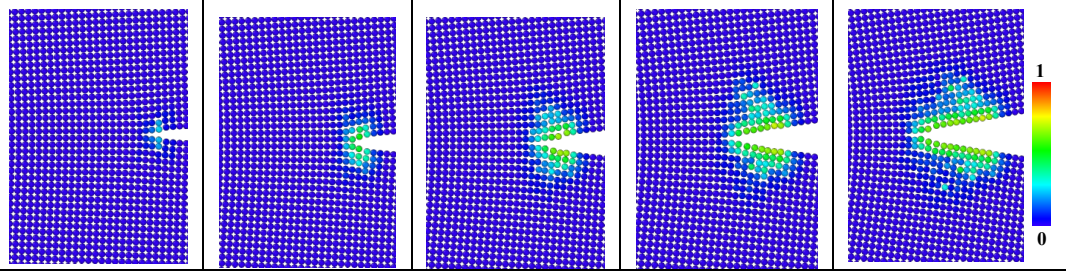				

In Taylor impact test [14], the specimen was a 31.75 mm long aluminum alloy 6061(T6) cylinder with the diameter of 6.35 mm. The system was discretized into 101988 material particles. The grid size was 0.3 mm and the horizon was 0.54 mm. The impact bar was moving towards a rigid wall at 289 m/s. The time step was chosen as 1×10^{-9}s. The ultimate configuration of the cylinder bar is presented in Fig. 5. Fig. 5(b) exhibits a typical mushroom head with a drum-like section near the impact face, in conformity to the EMU results. Material particles near the impact face are drastically mal-positioned with higher level of bond breakage. The normalized diameter at the impact face for the simulation is around 2.25 and the normalized length is around 0.85, in a satisfying conformity with experimental results.

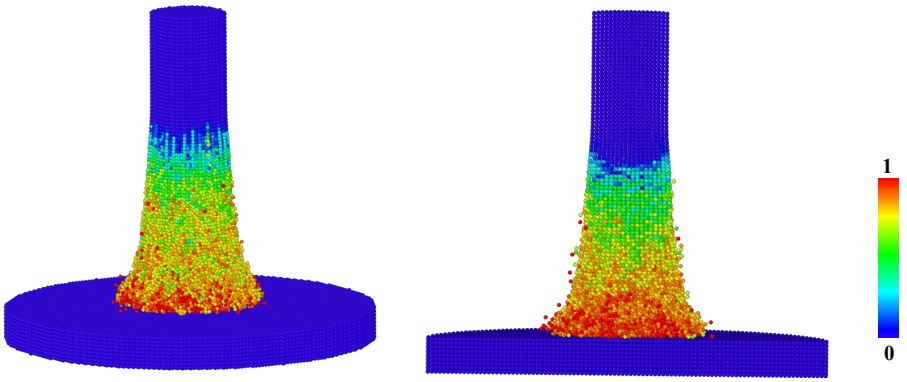

a) 3D version b) Middle plane

Fig. 5 The degree of bond breakage

Computation tasks are performed on a HP Z8 G4 work station, equipped with two Intel Xeon Gold 6154 CPUs. For all the benchmark tests afore-discussed, 16 processors are invoked in parallel. The CPU time per step per zone ranges from 0.5×10^{-6} s to 3×10^{-6} s. For a model composed of 5×10^{5} particles running for 5×10^{3} steps, at least 750 seconds are needed. The computational potential can still be further tapped by means of Carrera Unified Formulation and the CUF-based PD-FEM coupling schemes.

Summary

A two-step strategy is proposed to incorporate the BP theory and the Wang's ductile damage theory into OSB-PD framework. A unified elastoplastic peridynamics model is hereby established to simulate the full-course fracture behaviors for ductile materials in consideration of dislocation dynamics, void growth and coalescence. It retains the advantages from both unified constitutive theory and PD theory in predicting the natural development of plastic deformation and material failure. Its capabilities in describing material fractures are verified through a series of tension and impact simulations. The plastic deformation patterns, crack propagation paths and synchronic physical behaviors at different deformation stages have been reproduced to a satisfactory degree.

To optimize the present model, three-dimensional peridynamics can be further coupled with high-order two-dimensional finite elements based on local elasticity [15,16]. The collaboration between PD and CUF-based FEM [17] can retain the salient features of both local and nonlocal theories, which will bring new possibilities for the applications of the present two-step strategy.

References

[1] Li H, Fu MW, Lu J, Yang H. Ductile fracture: Experiments and computations. International Journal of Plasticity 2011;27:147–80. https://doi.org/10.1016/j.ijplas.2010.04.001.

[2] Silling SA, Madenci E. Editorial: The World Is Nonlocal. J Peridyn Nonlocal Model 2019;1:1–2. https://doi.org/10.1007/s42102-019-00009-7

[3] Erdogan Madenci, Atila Barut, Mehmet Dorduncu. Peridynamic Differential Operator for Numerical Analysis. Springer; 2019.

[4] Silling SA. Reformulation of elasticity theory for discontinuities and long-range forces. Journal of the Mechanics and Physics of Solids 2000;48:175–209. https://doi.org/10.1016/S0022-5096(99)00029-0

[5] Silling SA, Epton M, Weckner O, Xu J, Askari E. Peridynamic States and Constitutive Modeling. Journal of Elasticity 2007;88:151–84.https://doi.org/10.1007/s10659-007-9125-1

[6] Gu X, Zhang Q, Madenci E, Xia X. Possible causes of numerical oscillations in non-ordinary state-based peridynamics and a bond-associated higher-order stabilized model. Computer Methods in Applied Mechanics and Engineering 2019;357:112592. https://doi.org/10.1016/j.cma.2019.112592

[7] Javili A, Morasata R, Oterkus E, Oterkus S. Peridynamics review. Mathematics and Mechanics of Solids 2019;24:3714–39. https://doi.org/10.1177/1081286518803411

[8] Bodner SR. Review of a Unified Elastic—Viscoplastic Theory. In: Miller AK, editor. Unified Constitutive Equations for Creep and Plasticity, Dordrecht: Springer Netherlands; 1987, p. 273–301. https://doi.org/10.1007/978-94-009-3439-9_6

[9] Wang T-J. Unified CDM model and local criterion for ductile fracture—I. Unified CDM model for ductile fracture. Engineering Fracture Mechanics 1992;42:177–83. https://doi.org/10.1016/0013-7944(92)90289-Q

[10] Wang T-J. Unified CDM model and local criterion for ductile fracture—II. Ductile fracture local criterion based on the CDM model. Engineering Fracture Mechanics 1992;42:185–93. https://doi.org/10.1016/0013-7944(92)90290-U

[11] Madenci E, Oterkus S. Ordinary state-based peridynamics for plastic deformation according to von Mises yield criteria with isotropic hardening. Journal of the Mechanics and Physics of Solids 2016;86:192–219. https://doi.org/10.1016/j.jmps.2015.09.016

[12] Scapin M, Manes A. Behaviour of Al6061-T6 alloy at different temperatures and strain-rates: Experimental characterization and material modelling. Materials Science and Engineering: A 2018;734:318–28. https://doi.org/10.1016/j.msea.2018.08.011

[13] Xue Z, Pontin MG, Zok FW, Hutchinson JW. Calibration procedures for a computational model of ductile fracture. Engineering Fracture Mechanics 2010;77:492–509. https://doi.org/10.1016/j.engfracmech.2009.10.007

[14] Foster J. Dynamic crack initiation toughness: experiments and peridynamic modeling. 2009. https://doi.org/10.2172/1001000

[15] Pagani A, Carrera E. Coupling three-dimensional peridynamics and high-order one-dimensional finite elements based on local elasticity for the linear static analysis of solid beams and thin-walled reinforced structures. Int J Numer Methods Eng 2020;121:5066–81. https://doi.org/10.1002/nme.6510

[16] Pagani A, Enea M, Carrera E. Quasi-static fracture analysis by coupled three-dimensional peridynamics and high order one-dimensional finite elements based on local elasticity. Numerical Meth Engineering 2022;123:1098–113. https://doi.org/10.1002/nme.6890

[17] Carrera E, Cinefra M, Petrolo M, Zappino E. Finite element analysis of structures through unified formulation. Chichester, West Sussex: Wiley; 2014.